Research Article | Vol. 27, No. 11 | 27 May 2019 | OPTICS EXPRESS 15474
Optics EXPRESS

Correction of spectral distortion in two-dimensional electronic spectroscopy arising from the wedge-based delay line

RUIDAN ZHU,[1,2] SHUAI YUE,[1,2] HAO LI,[1,2] XUAN LENG,[1,2] ZHUAN WANG,[1] HAILONG CHEN,[1] AND YUXIANG WENG[1,2,*]

[1]*Beijing National Laboratory for Condensed Matter Physics, CAS Key Laboratory of Soft Matter Physics, Institute of Physics, Chinese Academy of Sciences, Beijing 100190, China*
[2]*University of Chinese Academy of Sciences, Beijing 100049, China*
[*]*yxweng@iphy.ac.cn*

Abstract: Unlike the probe wavelength, which is spectrally resolved by monochromator, the excitation wavelength in two-dimensional electronic spectroscopy is retrieved by means of Fourier transform of the interference signal introduced by the coherence delay time between the first and second excitation laser pulses. Hence, the calibration of delay lines would determine its accuracy. In this work, we showed that an inaccurate calibration factor of wedge-based delay line would result in a global peak shift and asymmetric spectral twists along the excitation axis. Both theoretical analysis and experiments have shown that such spectral distortions can be corrected by an accurately predetermined calibration factor. The relative accuracy of calibration factor reaches 3×10^{-5} in our setup. The dispersion effect of wedges also has been considered for the broadband excitation.

1. Introduction

Two-dimensional electronic spectroscopy (2DES) is an advanced spectroscopic tool for studying ultrafast energy and charge transfer possesses in condensed phase systems including biological light-harvesting systems [1–6], polymers and aggregates [7–10], as well as organic and inorganic semiconductors [11–14]. A 2DES map shows the correlation between the emission frequency (ω_3) and the initial excitation frequency (ω_1), directly revealing the coupling of different electronic states and energy relaxation pathways [15]. The excitation axis on 2D spectra is obtained by the Fourier transform of third-order nonlinear signals along the coherence time defined as the time delay between the first two excitation pulses. In order to control coherence delay time with sub-wavelength accuracy, there are three methods commonly used in 2DES setups: pulse shapers [16–18], a pair of movable transmitted wedges [19–23] and reflected mirrors [24–28]. These methods have their own advantages and disadvantages [29], among which the transmitted wedge-based delay line is a simple, compact and cost-effective way to provide attosecond time resolution, maintaining high optical phase stability between the pulses.

Although 2D spectroscopy obtains much more dynamic information than traditional pump-probe techniques, the reliable physical interpretation of each peak would depend exclusively on the quality of the spectra, i.e. free of unknown spectral distortions as much as possible. In general, the origins of spectral distortion, in most cases, are various for different geometrical configurations. Ogilvie *et al* analyzed the effects of laser pulse chirp on 2D spectra in a pump-probe geometry [30]. Jonas and Cundiff *et al* investigated the pulse propagation effects in a fully noncollinear geometry [31–33]. It is noted that the precise time zeros of the coherence time and the emission time (known as the phasing problem) are also essential to produce the correct 2D spectra in non-collinear 2DES. Recently, Jiang *et al* proposed new methods to improve the phasing procedure both in experiment and during data

#358554 https://doi.org/10.1364/OE.27.015474
Journal © 2019 Received 23 Jan 2019; revised 7 May 2019; accepted 7 May 2019; published 15 May 2019

Optics EXPRESS

post processing [34,35]. In addition, a finite laser bandwidth, as a spectral filter, would distort the corresponding coherence peak position as well as its line shape in 2DES [36–39]. In this paper we found another spectral twist phenomenon resulting from the calibration factor (CF) of the wedge-based coherence time (τ) delay line. The calibration factor (time delay versus translation distance) as a function of wedge position is determined by the wedge angle and refractive index, which also can be measured by spectral interference [19]. To the best of our knowledge, the spectral distortion in 2DES maps due to the inaccuracy of wedge angle and the dispersion have not been reported quantitatively before. Here, we present a typical-case study of the spectral distortion arising from the inaccurate CF of glass wedges in 2D maps of light-harvesting complex II (LHCII) in photosystem II of higher plants. Consequently, we obtained the CF values experimentally with a relative accuracy of 3×10^{-5} and provide a quantitative relation between the spectral shift and the deviation of CFs. Besides, a solution to dispersion correction is proposed to reduce the spectral distortion on 2D spectra.

2. Experimental setup

The schematic diagram of the 2DES setup is shown in Figs. 1(a) and 1(b). 35fs laser pulses were generated by Ti:sapphire laser system(Spitfire Ace, Spectra Physics) at a central wavelength of 800 nm (60 nm bandwidth), operating at an 1kHz repetition rate. The visible broadband light source was converted from 800 nm laser pulses by a home-built non-collinear optical parametric amplifier (NOPA), spanning the visible region (560-720 nm) with a full-width at half maximum (FWHM) bandwidth of 90 nm centered at 650 nm (See Fig. 1(c)). After pulse compression through a combination of chirped mirrors (Layertec) and a fused silica prism compressor, the resulting laser pulse could achieve a FWHM of 17fs.

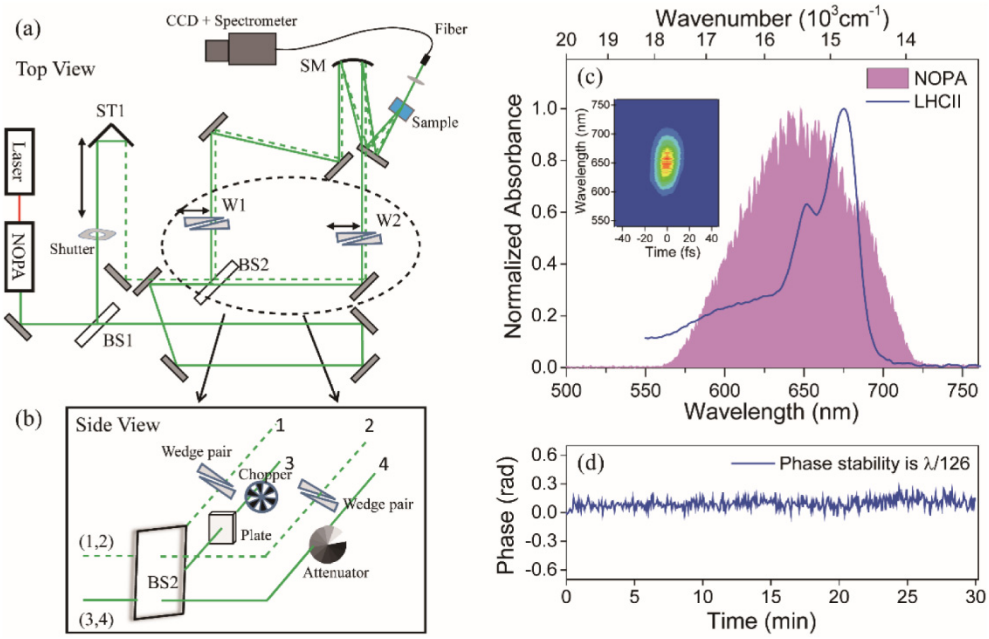

Fig. 1. Schematic diagram of 2DES experimental setup. (a) The setup with a top view. ST1 translation stage; BS1, 2 beam splitter; The time delays of beam 1 and 2 are tuned by glass wedge pairs W1 and W2, respectively; SM spherical mirror; (b) A side view for the circled part in (a); (c) The NOPA spectrum (magenta shaded) and the absorption spectrum (blue line) of LHCII at ambient temperature. The inset shows the measured transient grating frequency-resolved optical gating (TG-FROG) trace of the NOPA pulse measured at the sample position. The FWHM was measured to be 17 fs; (d) Phase stability of the heterodyned signals at 625 nm measured every 4 seconds over 30 minutes.

Optics EXPRESS

In our 2DES scheme, two broadband beam splitters (Layertec) were used to create four beams in a fully non-collinear geometry. After the first beam splitter (BS1), the input beam was separated into beam (1, 2) and beam (3, 4) respectively. Beam (1, 2) were delayed by a long-range translation stage ST1 (Newport) to introduce the population time (T) and the height of beam (3, 4) was lowered to be different from beam (1, 2) after four reflections. Then the second splitter (BS2) separated both beams into four beams resulting in a BOXCARS geometry. The inherent passive phase stability was achieved with a value of λ/120 in 30 minutes since pairs of pulses always passed through each reflective component [25], shown in Fig. 1(d). Two pairs glass wedges having a wedge angle of 1° (± 3′) (MT-Optics Inc), mounted on the other two short-range translation stages (25mm, 0.1μm minimum increment, Newport), were inserted to paths of beam 1 and 2 to control the coherence time between the excitation pulses 1 and 2, respectively. The fourth beam, as a local oscillator (LO), was attenuated by 3-4 orders in magnitude using a variable neutral density filter. After a spherical mirror (f = 300 mm), four beams in a 15mm × 15mm BOXCARS geometry were focused to a spot size of 200 μm at the sample position and photon echo signals along the direction of LO beam are collected by an EMCCD coupled spectrometer (SP2358, Princeton Instrument). In order to remove the scattering contribution and speed up the data acquisition, a shot-to-shot scheme was applied which has been reported in detailed previously [40]. All the 2DES measurements were performed with a pulse energy of less than 40 nJ. During data processing, 2D maps were phased using the projection slice theorem [41], in which two phase factors (ϕ: phase constant; t_c: time delay between beam 3 and the LO) were added to adjust the phase of 2D spectra to match the frequency-resolved pump-probe results.

Trimeric LHCII were isolated from spinach [42], dissolved in a buffer solution containing 0.03% β-dodecylmaltoside (β-DM) to an optical density (OD) at the Q_y band maximum (675 nm) of 0.3 in a 0.1-mm-thick closed cell. Each monomeric unit of native LHCII binds eight chlorophylls *a* (Chl *a*) and six chlorophylls *b* (Chl *b*) pigments, whose Q_y bands appear at 675 and 652 nm, respectively. The linear absorption spectrum of LHCII sample, shown in Fig. 1(c), was recorded at room temperature. The CF value we used is 26.6 fs/mm according to the nominal wedge angle (1°). Thus, the 2DES spectra of LHCII were collected by scanning the coherence time (τ) in the range of −106 – + 106 fs with a step size of 1.33 fs at each fixed population time.

3. Results and discussion

3.1. Spectral distortion in 2DES maps

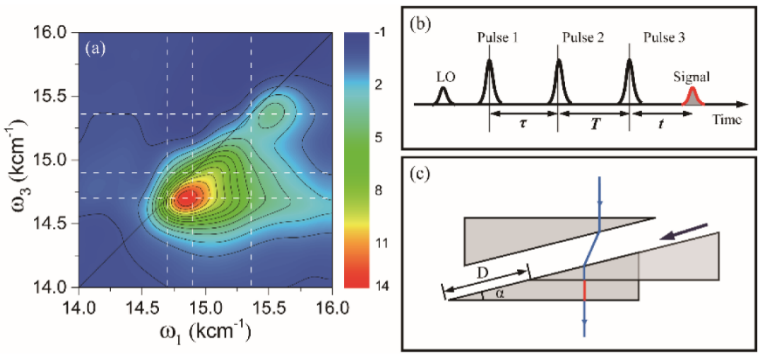

Fig. 2. (a) The as-acquired 2D map of LHCII at T = 200 fs. (b) Pulse sequence used in the 2DES setup. (c) A wedge-based delay line. Blue lines show the path of beam transmitting through the wedge pair and the red line indicates the optical path difference before and after the movement of wedge.

Optics EXPRESS

A typical as-acquired 2D map of LHCII at T = 200 fs is shown in Fig. 2(a). Viewed from the emission axis (ω_3), two peaks along to the diagonal predominantly correspond to the Q_y absorption band of Chl *b* and Chl *a* in LHCII, with the Chl *b* peak at 15360 cm^{-1} and two Chl *a* peaks (the main peak and the shoulder peak) at 14700 cm^{-1} and 14900 cm^{-1}, respectively. The cross peaks below the diagonal indicate the energy transfer from Chl *b* to Chl *a*, while the cross peak with negative amplitude located above the diagonal is due to the excited-state absorption from the Chl *a* state. These assignments have been discussed in the previous 2DES works on LHCII [43–47]. However, it is obvious that two peaks along the diagonal deviate from the diagonal collectively. Solvation effect or Stokes shift [41,48,49] is probably not so dominant as to generate such a large peak shift in this case since all the chlorophyll molecules are bound to the hydrophobic protein scaffold and the population time T is too short regarding to the solvation time. The laser spectrum covered the whole absorption band of LHCII so that the 2D signals are less affected by the effect of finite pulse width [36]. We further noted that the excitation energy of peaks mismatch with those in the absorption spectrum in Fig. 1(c), i.e. the spectral distortions with a global peak shift in the 2D map occur along the excitation axis. Since the excitation axis, obtained by the Fourier transform along the coherence delay time, is related to the CF of wedges, we analyze the factors of CF value in theory to explore whether if it is the possible origin of this spectral distortion.

3.2. Possible spectral distortions due to calibration factor

Two-dimensional electronic spectra are measured by exciting the sample in a certain phase-matched direction with a varied temporal sequence of three ultrashort pulses [41,50]. The third-order nonlinear response in a 2D spectrum can be described as:

$$S^{(3)}(\omega_1, T, \omega_3) = \iint S^{(3)}(\tau, T, t)\exp(i\omega_1\tau)\exp(i\omega_3 t)\,d\tau dt, \tag{1}$$

where the coherence time τ is defined as the time delay of the first two pulses. After the population time T, the third pulse induces an electric field signal with the emission time t in the propagation direction of the fourth (LO) pulse for optical heterodyne detection (See Fig. 2(b))

The coherence time delay can be created by a pair of glass wedges in an antiparallel orientation mounted on linear translation stages, shown in Fig. 2(c) [51]. When moving one of wedges with a certain distance (D) related to an initial position, the stage changes the optical path of a beam and creates a time delay $\Delta\tau = D\,(n\text{-}1)\,\sin\alpha/c$ for small wedge angle (α). n is the refractive index of wedges (typically fused silica) and c is the velocity of light in vacuum. Thus, the CF of wedges is defined as:

$$k = \frac{\Delta\tau}{D} = (n-1)\sin\alpha / c. \tag{2}$$

Assuming that the refractive index is wavelength-independent in the range of laser spectrum and the nominal wedge angle α is 1°, the value of k is approximately 26.6 fs/mm as used in Fig. 2(a). However, because of the manufacturing technical limit of wedges, an inaccurate wedge angle (e.g. error with ± 3′) may introduce a distinct deviation (± 1.3 fs/mm) for the CF.

In order to obtain the quantitative influence of inaccurate k' value on 2D maps, we assume a two-level system with a transition energy of ω_0 and its third-order response can be described simply as $\exp(-i\omega_0\tau)$. Since CF is only related to the coherence time, here we neglect the integral term of emission axis ω_3. Then, the Fourier transform along the excitation axis with inaccurate coherence time (τ') can be written as:

Optics EXPRESS

$$S^{(3)}(\omega_1)=\int \exp(-i\omega_0\tau)\exp\left(i\omega_1\frac{k'}{k}\tau\right)d\tau=\frac{k}{k'}\delta\left(\omega_1-\frac{k}{k'}\omega_0\right). \quad (3)$$

From the expression of (3), it is clear that the resulting excitation energy in 2D map differs from the initial position (ω_0). The relative spectral shift can be described as:

$$\frac{\Delta\omega}{\omega_0}=\frac{k-k'}{k'}\approx-\frac{\Delta k}{k}. \quad (4)$$

It is obvious that the relative spectral shift is proportional to the relative error of CF. When the inaccurate CF (k') is larger than the actual value (k), the peak in 2DES maps has a global red shift along the excitation axis. When k' is less than k, there is a blue shift along the excitation axis. Given ω_0 = 16000 cm^{-1}, k = 26.6 fs/mm and Δk = 0.2 fs/mm, the peak shift can be estimated to be 120 cm^{-1}, which is misinterpreted easily as the solvation effect or Stokes shift on 2D spectra. Thus, it can be seen that a minor deviation of wedge angle would lead to an apparent spectral distortion as discussed above. Therefore, an accurate calibration and correction must be taken to reduce this distortion. It is noted that these peak shifts cannot be corrected by phasing through the projection slice theorem because CF value only dominates the step size of coherence time.

3.3. Calibration and correction

Spectral interferometry is an efficient measurement for the CF of glass wedge, which was first proposed by Brixner *et al* [19]. First, we place a 100 μm diameter pinhole at the sample position and block the third beam and LO beam. Then both beams 1 and 2 pass through the pinhole and create a spectral interference pattern (See Fig. 3(a)) when a glass wedge is moved in one of the beams. Fourier transform and a Hamming window are used to extract the oscillation component at each detected wavelength, shown in Fig. 3(b). Finally, the phases of the oscillation are retrieved by inverse Fourier transform and the CF can be determined by fitting the slope of the unwrapped phase vs translation distance at each wavelength, shown in Fig. 3(c). In addition, the residue of phase fitting as shown in Fig. 3(c) could be used to estimate the surface roughness of wedges [52].

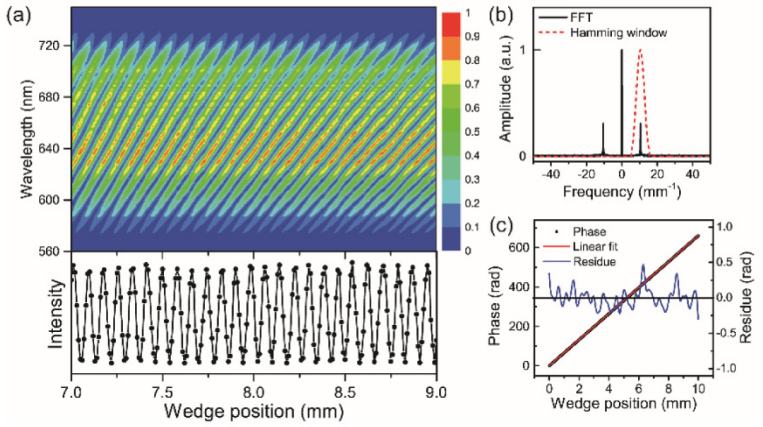

Fig. 3. Wedge calibration by spectral interferometry. (a) Top: spectral interference pattern of beam 1 and 2 by moving the position of the wedge 1 with a step of 0.01 mm. Bottom: the temporal oscillation at 650 nm wavelength. (b) Extraction of the temporal oscillation component. The black curve shows the Fourier transform result and the red dashed line is the Hamming window to filter the oscillating term. (c) The linear fitting (red line) of the unwrapped phase (black point) after the inverse Fourier transform for the data filtered in (b). The residue of phase fitting is also indicated as blue line.

Optics EXPRESS

In our measurement, each wedge is moved with a step of 0.01 mm over 10 mm to reduce the influence from the error of the wedge surface flatness. Figure 3(a) shows the partial spectral interference pattern recorded from the wedge 1. Due to the excellent phase stability in our 2DES setup, the relative standard deviation $\Delta k/k$ in our calibration is maintained below 3×10^{-5}, corresponding to a possible spectral shift $\Delta\omega$ of 0.5 cm^{-1} at 650 nm wavelength, which indicates the calibration of CFs is accurate and reliable. The final CF results are obtained in Fig. 4, which are dependent on the wavelength. Noted that the curves of wedge 1 and 2 correspond to the CFs of rephasing and nonrephasing spectra respectively. The difference of CF between wedge 1 and 2 is less than 0.05 fs/mm, indicating that both wedges are nearly identical. However, the variation of each CF is approximately 0.3 fs/mm from 560 nm to 760 nm. The wavelength dependence of CF originates from the refractive index of glass wedges $n(\omega)$ according to Eq. (2). For comparison, we utilize the three-term Sellmeier equation [53] to describe the material dispersion curve $n(\omega)$ and the theoretical CF curves are calculated with different wedge angles, shown as dashed lines in Fig. 4. The measured wavelength dependence of CFs is consistent with the calculated ones. Therefore, the actual wedge angles we calibrated are estimated to be 1° + 0.6′. Although the deviation from the nominal angle is much less than the given standard error (± 3′), it could lead to spectral distortions as discussed below. Because the main spectral signals of LHCII are only located in the 650 – 700 nm, the wavelength-dependent CF curves, for the sake of discussion, are substituted for an averaged CF value (k_A = 26.84 fs/mm) to study the spectral distortion effect. The wavelength dependence will be taken account of in the last part.

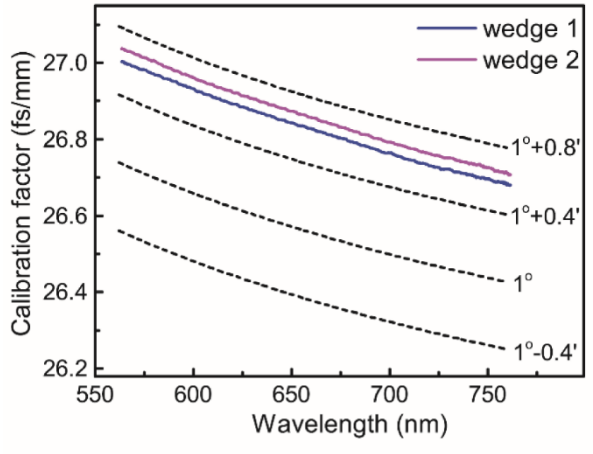

Fig. 4. Wavelength dependence of the calibration factor. The solid curves show the calibration factors of wedge 1 (blue) and wedge 2 (magenta) corresponding to the first two excitation beams respectively and the dashed curves indicate the calculated results according to the Eq. (2) with different wedge angles.

Optics EXPRESS

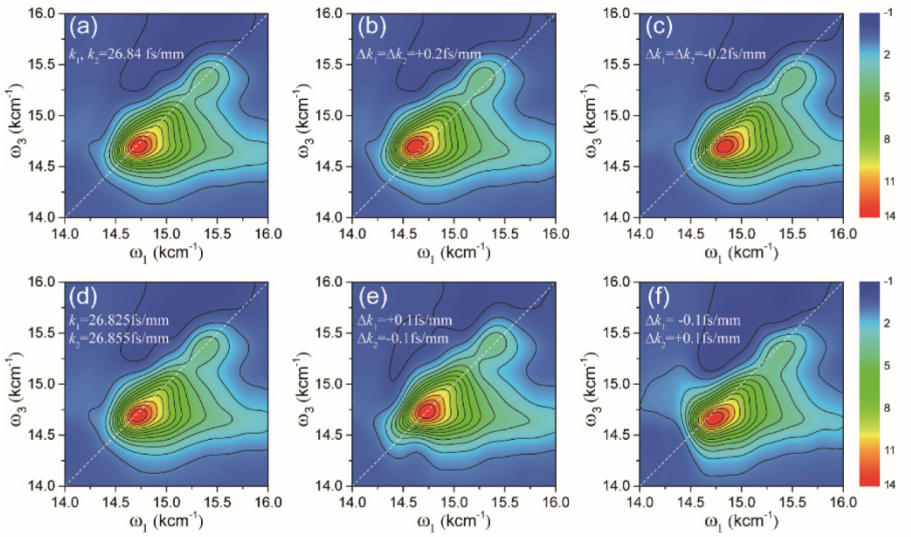

Fig. 5. Spectral distortions in 2DES of LHCII caused by different CF values at T = 200 fs. (a) The same wavelength-averaged CF value for both k_1 and k_2 according to calibration results in Fig. 4; (b) k value with an error of + 0.2 fs/mm; (c) k value with an error of –0.2 fs/mm. (d) The individual averaged k value for k_1 and k_2 according to Fig. 4; (e) k_1 with the error of + 0.1 fs/mm and k_2 with the error of –0.1 fs/mm; (f) the opposite case of (e). The diagonal lines are plotted as white dashed lines in 2D spectra.

To demonstrate the CF effect on the spectra, 2D maps of LHCII having different CF values are constructed under the same experimental condition at the fixed population time (T = 200 fs), as shown in Fig. 5. In the Fig. 5(a), the same measured CF value (k = 26.84 fs/mm) is used for both rephasing and nonrephasing spectra. Two Chl *a*/*b* diagonal peaks, as expected, are relocated along the diagonal and the excitation energy also matches those in the absorption spectrum of LHCII, from which we can infer that the spectrum is appropriately corrected. Figures 5(c) and 5(d) show distorted spectra with an introduced error in calibration factor of ± 0.2 fs/mm respectively. All the peaks are either red-shift in Fig. 5(b) or blue-shift in Fig. 5(c) with a deviation about 110 cm^{-1}, which are in accordance with the relation in Eq. (4).

However, it should be noted that the spectral shape may undergo more complicated twists when variations in k values for rephasing and nonrephasing spectrum are different since a pure absorptive spectrum is the sum of both real-part rephasing and nonrephasing spectra. In Figs. 5(d)−5(f), three additional 2D spectra are provided in which CF values of the rephasing and nonrephasing spectra are treated individually with a slightly different modification. Clearly, the spectrum with the actual wavelength-averaged values (k_1 = 26.825 fs/mm and k_2 = 26.855 fs/mm) in Fig. 5(d) has no apparent distinction from that in Fig. 5(a), indicating that the spectrum in Fig. 5(d) is free of distortion and that the error of ± 0.02 fs/mm is small enough to neglect the resulted spectral distortion. However, by introducing a positive error of 0.1 fs/mm to the rephasing spectrum and a negative error to the nonrephasing, significant spectral twist can be produced in Fig. 5(e) and vice versa in Fig. 5(f). Because rephasing and nonrephasing spectra undergo peak shifts which are equal in magnitude but opposite in direction along the excitation axis, the resulting 2D absorptive spectra show slightly larger spectral broadening along ω_1 axis. If the error of CF became larger, the spectral broadening would be distinct enough to affect the measurement of homogeneous broadening on the diagonal peaks. In particular, an obvious peak shift in Fig. 5(f) with respect to that of Fig. 5(e), can be easily mixed up with Fig. 5(c). This precludes the attempt to refine an accurate

CF without calibration from the global peak shift along the excitation axis with respect to the absorption spectrum.

In Section 3.2, we have obtained a quantitative relation between the spectral shift and the error in the calibration factor as shown in Eq. (4). Since the pure absorptive spectrum is the sum of the rephasing and nonrephasing spectrum, the spectral shift is governed by the maximum of distortion from either the rephasing or non-rephasing spectrum. Based on Eq. (4), the spectral shift in the pure absorptive spectrum is defined as:

$$\left|\frac{\Delta\omega}{\omega}\right| \le \max\left(\frac{|\Delta k_1|}{k_1}, \frac{|\Delta k_2|}{k_2}\right), \tag{5}$$

which is verified in Figs. 5(b), 5(c), 5(e) and 5(f).

Finally, we also verify the CF effect with wavelength dependence by introducing different coherence time series for each excitation wavelength (λ_m, m is the number of pixels), given by

$$\tau_m(i) = k(\lambda_m)x(i), \tag{6}$$

where $x(i)$ is the fixed wedge displacement series for every scanning. Here, the actual CF curves $k_1(\lambda)$ and $k_2(\lambda)$ for both rephasing and nonrephasing data are considered in the resulting 2D spectrum, shown in Fig. 6(a). In order to distinguish the difference before and after modification, a comparison of slices from 2D spectra in Fig. 6(a) (solid curves) and Fig. 5(a) (dashed curves) taken along the emission axis at the 14700 cm^{-1} (blue line) and 15360 cm^{-1} (red line) is shown in Fig. 6(b). The averaged CF values result in a slight broadening along excitation axis but no evident shape distortion compared with Fig. 6(a) so that the wavelength dependence of CF is negligible for our 2DES measurements. One should note that in the given excitation range as shown in Fig. 6, $k(\lambda)$ only gives rise to a change in CF about 0.15 fs/mm. When a broader spectral range is involved, the corresponding $k(\lambda)$ would lead to a change of CF larger than 0.2 fs/mm, and then the wavelength-dependent CF should be used instead of the wavelength-averaged one.

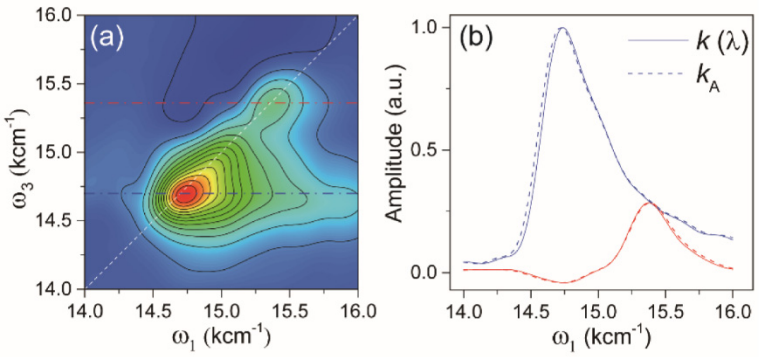

Fig. 6. (a) Spectral correction according to the wavelength-dependent $k(\lambda)$ curves. (b) The comparison of slices between Figs. 6(a) and 5(a) taken along two dash dot lines in (a). The blue (red) color indicates the detection energy position of Chl *a* (Chl *b*) and the solid (dashed) line indicates the result from the *k* value with (without) wavelength dependence.

Other minor factors may exist which lead to distortion effects along the excitation axis. For example, Augulis *et al* have proposed a calibration method [52] to eliminate the spectral phase error from surface thickness variations of wedges. It is no doubt that poor surface roughness of wedges will result in shape twists, while the measured CF value is insensitive to the wedge surface because linear fitting is taken to neglect the minor phase error during the procedure in Fig. 3(c). Thus, the deviation of CF value would cause a global peak shift as above discussion, but surface roughness would only lead to local peak twists in 2D maps.

Optics EXPRESS

4. Conclusion

We have presented the theoretical analysis and 2DES implementation to explore effects of the inaccurate calibration factor for wedge-based delay lines leading to the distortion of 2D maps. Using a simple two-level system, we find the quantitative relation between the accuracy of calibration factors and the spectral shift along the excitation axis in 2D spectra. The as-acquired and corrected 2DES maps of LHCII provide a typical example. A relative accuracy in calibration factor of 3×10^{-5} is obtained to correct our spectra. Besides the global peak shift, more complex spectral twists may arise, especially when the deviations between wedge 1 and 2 are different or of opposite sign. Furthermore, after dispersion correction it is found that dispersion effects on the calibration factor make little contribution for spectral twist in 2DES measurements, but probably should be considered during data processing using Eq. (6) when a larger excitation bandwidth is involved in 2D spectra.

Funding

National Key R&D Program of China (2018YFA0208700); National Natural Science Foundation of China (NSFC) (21433014 and 11721404); Chinese Academy of Sciences Frontier Science Key Programs (QYZDJ-SSW-SYS017); National Key Foundation for Developing Scientific Instrument (2013YQ030595).

Disclosures

The authors declare that there are no conflicts of interest related to this article.

References

1. G. S. Engel, T. R. Calhoun, E. L. Read, T. K. Ahn, T. Mancal, Y. C. Cheng, R. E. Blankenship, and G. R. Fleming, "Evidence for wavelike energy transfer through quantum coherence in photosynthetic systems," Nature **446**(7137), 782–786 (2007).
2. F. D. Fuller, J. Pan, A. Gelzinis, V. Butkus, S. S. Senlik, D. E. Wilcox, C. F. Yocum, L. Valkunas, D. Abramavicius, and J. P. Ogilvie, "Vibronic coherence in oxygenic photosynthesis," Nat. Chem. **6**(8), 706–711 (2014).
3. E. Romero, R. Augulis, V. I. Novoderezhkin, M. Ferretti, J. Thieme, D. Zigmantas, and R. van Grondelle, "Quantum Coherence in Photosynthesis for Efficient Solar Energy Conversion," Nat. Phys. **10**(9), 676–682 (2014).
4. J. C. Dean, T. Mirkovic, Z. S. D. Toa, D. G. Oblinsky, and G. D. Scholes, "Vibronic Enhancement of Algae Light Harvesting," Chem **1**(6), 858–872 (2016).
5. H. G. Duan, V. I. Prokhorenko, R. J. Cogdell, K. Ashraf, A. L. Stevens, M. Thorwart, and R. J. D. Miller, "Nature does not rely on long-lived electronic quantum coherence for photosynthetic energy transfer," Proc. Natl. Acad. Sci. U.S.A. **114**(32), 8493–8498 (2017).
6. S. Yue, Z. Wang, X. Leng, R. D. Zhu, H. L. Chen, and Y. X. Weng, "Coupling of multi-vibrational modes in bacteriochlorophyll a in solution observed with 2D electronic spectroscopy," Chem. Phys. Lett. **683**, 591–597 (2017).
7. E. Collini and G. D. Scholes, "Coherent intrachain energy migration in a conjugated polymer at room temperature," Science **323**(5912), 369–373 (2009).
8. J. Lim, D. Paleček, F. Caycedo-Soler, C. N. Lincoln, J. Prior, H. von Berlepsch, S. F. Huelga, M. B. Plenio, D. Zigmantas, and J. Hauer, "Vibronic origin of long-lived coherence in an artificial molecular light harvester," Nat. Commun. **6**(1), 7755 (2015).
9. A. De Sio, F. Troiani, M. Maiuri, J. Réhault, E. Sommer, J. Lim, S. F. Huelga, M. B. Plenio, C. A. Rozzi, G. Cerullo, E. Molinari, and C. Lienau, "Tracking the coherent generation of polaron pairs in conjugated polymers," Nat. Commun. **7**(1), 13742 (2016).
10. V. Butkus, J. Alster, E. Bašinskaitė, R. N. Augulis, P. Neuhaus, L. Valkunas, H. L. Anderson, D. Abramavicius, and D. Zigmantas, "Discrimination of Diverse Coherences Allows Identification of Electronic Transitions of a Molecular Nanoring," J. Phys. Chem. Lett. **8**(10), 2344–2349 (2017).
11. J. M. Richter, F. Branchi, F. Valduga de Almeida Camargo, B. Zhao, R. H. Friend, G. Cerullo, and F. Deschler, "Ultrafast carrier thermalization in lead iodide perovskite probed with two-dimensional electronic spectroscopy," Nat. Commun. **8**(1), 376 (2017).
12. E. Cassette, R. D. Pensack, B. Mahler, and G. D. Scholes, "Room-temperature exciton coherence and dephasing in two-dimensional nanostructures," Nat. Commun. **6**(1), 6086 (2015).
13. T. Stoll, F. Branchi, J. Réhault, F. Scotognella, F. Tassone, I. Kriegel, and G. Cerullo, "Two-Dimensional Electronic Spectroscopy Unravels sub-100 fs Electron and Hole Relaxation Dynamics in Cd-Chalcogenide Nanostructures," J. Phys. Chem. Lett. **8**(10), 2285–2290 (2017).

Optics EXPRESS

14. D. M. Monahan, L. Guo, J. Lin, L. Dou, P. Yang, and G. R. Fleming, "Room-Temperature Coherent Optical Phonon in 2D Electronic Spectra of $CH_3NH_3PbI_3$ Perovskite as a Possible Cooling Bottleneck," J. Phys. Chem. Lett. **8**(14), 3211–3215 (2017).
15. T. Brixner, J. Stenger, H. M. Vaswani, M. Cho, R. E. Blankenship, and G. R. Fleming, "Two-dimensional spectroscopy of electronic couplings in photosynthesis," Nature **434**(7033), 625–628 (2005).
16. J. A. Myers, K. L. Lewis, P. F. Tekavec, and J. P. Ogilvie, "Two-color two-dimensional Fourier transform electronic spectroscopy with a pulse-shaper," Opt. Express **16**(22), 17420–17428 (2008).
17. D. B. Turner, K. W. Stone, K. Gundogdu, and K. A. Nelson, "Invited article: The coherent optical laser beam recombination technique (COLBERT) spectrometer: coherent multidimensional spectroscopy made easier," Rev. Sci. Instrum. **82**(8), 081301 (2011).
18. D. Keusters, H.-S. Tan, and W. S. Warren, "Role of pulse phase and direction in two-dimensional optical spectroscopy," J. Phys. Chem. A **103**(49), 10369–10380 (1999).
19. T. Brixner, T. Mancal, I. V. Stiopkin, and G. R. Fleming, "Phase-stabilized two-dimensional electronic spectroscopy," J. Chem. Phys. **121**(9), 4221–4236 (2004).
20. T. Brixner, I. V. Stiopkin, and G. R. Fleming, "Tunable two-dimensional femtosecond spectroscopy," Opt. Lett. **29**(8), 884–886 (2004).
21. A. Nemeth, J. Sperling, J. Hauer, H. F. Kauffmann, and F. Milota, "Compact phase-stable design for single- and double-quantum two-dimensional electronic spectroscopy," Opt. Lett. **34**(21), 3301–3303 (2009).
22. R. Augulis and D. Zigmantas, "Two-dimensional electronic spectroscopy with double modulation lock-in detection: enhancement of sensitivity and noise resistance," Opt. Express **19**(14), 13126–13133 (2011).
23. D. Brida, C. Manzoni, and G. Cerullo, "Phase-locked pulses for two-dimensional spectroscopy by a birefringent delay line," Opt. Lett. **37**(15), 3027–3029 (2012).
24. M. L. Cowan, J. P. Ogilvie, and R. J. D. Miller, "Two-dimensional spectroscopy using diffractive optics based phased-locked photon echoes," Chem. Phys. Lett. **386**(1–3), 184–189 (2004).
25. U. Selig, F. Langhojer, F. Dimler, T. Löhrig, C. Schwarz, B. Gieseking, and T. Brixner, "Inherently phase-stable coherent two-dimensional spectroscopy using only conventional optics," Opt. Lett. **33**(23), 2851–2853 (2008).
26. J. D. Hybl, A. Albrecht Ferro, and D. M. Jonas, "Two-dimensional Fourier transform electronic spectroscopy," J. Chem. Phys. **115**(14), 6606–6622 (2001).
27. H. Zheng, J. R. Caram, P. D. Dahlberg, B. S. Rolczynski, S. Viswanathan, D. S. Dolzhnikov, A. Khadivi, D. V. Talapin, and G. S. Engel, "Dispersion-free continuum two-dimensional electronic spectrometer," Appl. Opt. **53**(9), 1909–1917 (2014).
28. W. Zhu, R. Wang, C. Zhang, G. Wang, Y. Liu, W. Zhao, X. Dai, X. Wang, G. Cerullo, S. Cundiff, and M. Xiao, "Broadband two-dimensional electronic spectroscopy in an actively phase stabilized pump-probe configuration," Opt. Express **25**(18), 21115–21126 (2017).
29. F. D. Fuller and J. P. Ogilvie, "Experimental implementations of two-dimensional fourier transform electronic spectroscopy," Annu. Rev. Phys. Chem. **66**(1), 667–690 (2015).
30. P. F. Tekavec, J. A. Myers, K. L. Lewis, F. D. Fuller, and J. P. Ogilvie, "Effects of chirp on two-dimensional Fourier transform electronic spectra," Opt. Express **18**(11), 11015–11024 (2010).
31. H. Li, A. P. Spencer, A. Kortyna, G. Moody, D. M. Jonas, and S. T. Cundiff, "Pulse propagation effects in optical 2D Fourier-transform spectroscopy: experiment," J. Phys. Chem. A **117**(29), 6279–6287 (2013).
32. B. Cho, M. K. Yetzbacher, K. A. Kitney, E. R. Smith, and D. M. Jonas, "Propagation and beam geometry effects on two-dimensional fourier transform spectra of multilevel systems," J. Phys. Chem. A **113**(47), 13287–13299 (2009).
33. M. K. Yetzbacher, N. Belabas, K. A. Kitney, and D. M. Jonas, "Propagation, beam geometry, and detection distortions of peak shapes in two-dimensional Fourier transform spectra," J. Chem. Phys. **126**(4), 044511 (2007).
34. Y. Zhang, T. M. Yan, and Y. H. Jiang, "Precise phase determination with the built-in spectral interferometry in two-dimensional electronic spectroscopy," Opt. Lett. **41**(17), 4134–4137 (2016).
35. Q. Meng, Y. Zhang, T. M. Yan, and Y. H. Jiang, "Post-processing phase-correction algorithm in two-dimensional electronic spectroscopy," Opt. Express **25**(6), 6644–6652 (2017).
36. R. Tempelaar, A. Halpin, P. J. Johnson, J. Cai, R. S. Murphy, J. Knoester, R. J. D. Miller, and T. L. Jansen, "Laser-Limited Signatures of Quantum Coherence," J. Phys. Chem. A **120**(19), 3042–3048 (2016).
37. F. V. de A Camargo, L. Grimmelsmann, H. L. Anderson, S. R. Meech, and I. A. Heisler, "Resolving Vibrational from Electronic Coherences in Two-Dimensional Electronic Spectroscopy: The Role of the Laser Spectrum," Phys. Rev. Lett. **118**(3), 033001 (2017).
38. X. Leng, S. Yue, Y.-X. Weng, K. Song, and Q. Shi, "Effects of finite laser pulse width on two-dimensional electronic spectroscopy," Chem. Phys. Lett. **667**, 79–86 (2017).
39. T. N. Do, M. F. Gelin, and H.-S. Tan, "Simplified expressions that incorporate finite pulse effects into coherent two-dimensional optical spectra," J. Chem. Phys. **147**(14), 144103 (2017).
40. S. Yue, Z. Wang, X. C. He, G. B. Zhu, and Y. X. Weng, "Construction of the Apparatus for Two Dimensional Electronic Spectroscopy and Characterization of the Instrument," Chin. J. Chem. Phys. **28**(4), 509–517 (2015).
41. D. M. Jonas, "Two-dimensional femtosecond spectroscopy," Annu. Rev. Phys. Chem. **54**(1), 425–463 (2003).
42. S. Caffarri, R. Croce, J. Breton, and R. Bassi, "The major antenna complex of photosystem II has a xanthophyll binding site not involved in light harvesting," J. Biol. Chem. **276**(38), 35924–35933 (2001).

Optics EXPRESS

43. G. S. Schlau-Cohen, T. R. Calhoun, N. S. Ginsberg, E. L. Read, M. Ballottari, R. Bassi, R. van Grondelle, and G. R. Fleming, "Pathways of energy flow in LHCII from two-dimensional electronic spectroscopy," J. Phys. Chem. B **113**(46), 15352–15363 (2009).
44. K. L. Wells, P. H. Lambrev, Z. Zhang, G. Garab, and H. S. Tan, "Pathways of energy transfer in LHCII revealed by room-temperature 2D electronic spectroscopy," Phys. Chem. Chem. Phys. **16**(23), 11640–11646 (2014).
45. H. G. Duan, A. L. Stevens, P. Nalbach, M. Thorwart, V. I. Prokhorenko, and R. J. D. Miller, "Two-dimensional electronic spectroscopy of light-harvesting complex ii at ambient temperature: a joint experimental and theoretical study," J. Phys. Chem. B **119**(36), 12017–12027 (2015).
46. C. Ramanan, M. Ferretti, H. van Roon, V. I. Novoderezhkin, and R. van Grondelle, "Evidence for coherent mixing of excited and charge-transfer states in the major plant light-harvesting antenna, LHCII," Phys. Chem. Chem. Phys. **19**(34), 22877–22886 (2017).
47. X. Leng, Y. M. Yan, R. D. Zhu, K. Song, Y. X. Weng, and Q. Shi, "Simulation of the two-dimensional electronic spectroscopy and energy transfer dynamics of light-harvesting complex ii at ambient temperature," J. Phys. Chem. B **122**(17), 4642–4652 (2018).
48. J. D. Hybl, A. Yu, D. A. Farrow, and D. M. Jonas, "Polar solvation dynamics in the femtosecond evolution of two-dimensional Fourier transform spectra," J. Phys. Chem. A **106**(34), 7651–7654 (2002).
49. A. Nemeth, F. Milota, T. Mančal, V. Lukeš, H. F. Kauffmann, and J. Sperling, "Vibronic modulation of lineshapes in two-dimensional electronic spectra," Chem. Phys. Lett. **459**(1–6), 94–99 (2008).
50. Y. X. Weng, "Detection of electronic coherence via two-dimensional electronic spectroscopy in condensed phase," Chin. J. Chem. Phys. **31**(2), 135–151 (2018).
51. E. Harel, A. F. Fidler, and G. S. Engel, "Single-shot gradient-assisted photon echo electronic spectroscopy," J. Phys. Chem. A **115**(16), 3787–3796 (2011).
52. R. Augulis and D. Zigmantas, "Detector and dispersive delay calibration issues in broadband 2D electronic spectroscopy," J. Opt. Soc. Am. B **30**(6), 1770–1774 (2013).
53. I. H. Malitson, "Interspecimen comparison of the refractive index of fused silica," J. Opt. Soc. Am. **55**(10), 1205–1209 (1965).